



HAL
open science

Enhanced permeability dielectric FeCo/Al₂O₃ multilayer thin films with tailored properties deposited by magnetron sputtering on silicon

Claudiu V. Falub, Srinivas V. Pietambaram, Oguz Yildirim, Mojmir Meduna, Ondrej Caha, Rachid Hida, Xue Zhao, Jan Ambrosini, Hartmut Rohrmann, Hans J. Hug

► **To cite this version:**

Claudiu V. Falub, Srinivas V. Pietambaram, Oguz Yildirim, Mojmir Meduna, Ondrej Caha, et al.. Enhanced permeability dielectric FeCo/Al₂O₃ multilayer thin films with tailored properties deposited by magnetron sputtering on silicon. AIP Advances, 2019, 9 (3), 10.1063/1.5079477 . cea-02186483

HAL Id: cea-02186483

<https://cea.hal.science/cea-02186483v1>

Submitted on 30 Sep 2024

HAL is a multi-disciplinary open access archive for the deposit and dissemination of scientific research documents, whether they are published or not. The documents may come from teaching and research institutions in France or abroad, or from public or private research centers.



L'archive ouverte pluridisciplinaire **HAL**, est destinée au dépôt et à la diffusion de documents scientifiques de niveau recherche, publiés ou non, émanant des établissements d'enseignement et de recherche français ou étrangers, des laboratoires publics ou privés.



Distributed under a Creative Commons Attribution 4.0 International License

Enhanced permeability dielectric FeCo/Al₂O₃ multilayer thin films with tailored properties deposited by magnetron sputtering on silicon

Special Collection: [2019 Joint MMM-Intermag Conference](#)

Claudiu V. Falub  ; Srinivas V. Pietambaram; Oguz Yildirim; Mojmír Meduňa; Ondrej Caha; Rachid Hida; Xue Zhao; Jan Ambrosini; Hartmut Rohrmann; Hans J. Hug



AIP Advances 9, 035243 (2019)

<https://doi.org/10.1063/1.5079477>



Articles You May Be Interested In

Disorder-modulated microwave absorption properties of carbon-coated FeCo nanocapsules

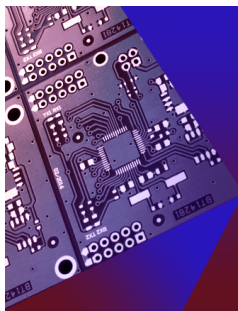
J. Appl. Phys. (February 2014)

Synthesis of high magnetization FeCo alloys prepared by a modified polyol process

J. Appl. Phys. (March 2011)

Fabrication and characterization of IrMn/PtMn/PtCr/PtMn antiferromagnets in terms of the role of each layer

AIP Advances (December 2019)



APL Electronic Devices

Fostering connections across multiple disciplines
in the broad electronics community

Now Open for Submissions



Enhanced permeability dielectric FeCo/Al₂O₃ multilayer thin films with tailored properties deposited by magnetron sputtering on silicon

Cite as: AIP Advances 9, 035243 (2019); doi: 10.1063/1.5079477

Presented: 18 January 2019 • Submitted: 31 October 2018 •

Accepted: 4 March 2019 • Published Online: 21 March 2019



Claudiu V. Falub,^{1,a)} Srinivas V. Pietambaram,² Oguz Yildirim,³ Mojmir Meduňa,^{4,5} Ondrej Caha,^{4,5} Rachid Hida,⁶ Xue Zhao,^{1,3} Jan Ambrosini,¹ Hartmut Rohrmann,¹ and Hans J. Hug³

AFFILIATIONS

¹Evatec AG, Hauptstrasse 1a, CH-9477 Trübbach, Switzerland

²Intel Corporation, W. Chandler Blvd. 5000, Chandler, AZ 85226, United States

³Nanoscale Materials Science, Empa, Überlandstrasse 129, CH-8600 Dübendorf, Switzerland

⁴Department of Condensed Matter Physics, Masaryk University, Kotlářská 2, CZ-60200 Brno, Czech Republic

⁵CEITEC, Masaryk University, Kamenice 5, CZ-60200 Brno, Czech Republic

⁶Univ. Grenoble Alpes, CEA-LETI, Rue des Martyrs 17, FR-38054 Grenoble, France

Note: This paper was presented at the 2019 Joint MMM-Intermag Conference.

^{a)}**Corresponding author:** Claudiu.Falub@evatecnet.com

ABSTRACT

We have studied the structural and magnetic properties of enhanced-permeability-dielectric FeCo/Al₂O₃-multilayer thin films deposited on 8"-Si wafers in an industrial magnetron sputtering system. The EPD-multilayers consist of 25 periods of alternating nanometer-thick FeCo-layers deposited by DC sputtering from a Fe₆₀Co₄₀ target and Al₂O₃-interlayers deposited by RF sputtering from an Al₂O₃ target. We tuned the magnetic properties of these thin films by varying the thickness of FeCo-layers from 1.1nm to 2.1nm, while the thickness of Al₂O₃-interlayers remained unchanged (3.5nm). The formation of layers of disconnected FeCo-nanoparticles separated by an Al₂O₃-matrix was revealed by grazing incidence small angle X-ray-scattering. Further insight into the microstructure of these layers was obtained from X-ray-reflectivity, highly asymmetric-X-ray-diffraction and non-coplanar grazing-incidence-diffraction. The Fe/Co ratio in the FeCo-layers obtained from X-ray-fluorescence measurements was (59±1)/(41±1), which is in very good agreement with the nominal value in the Fe₆₀Co₄₀ target. Using the standing wave technique we found that most of the Fe and Co atoms were located inside the polycrystalline grains, except for a small fraction that diffused into the Al₂O₃-matrix, and that the thinner the FeCo-layers thickness the higher the fraction of diffused atoms with respect to those in the grains. Zero-field-cooled, field-cooled, and hysteresis (*B-H*) and (*M-H*) measurements showed that the FeCo/Al₂O₃-multilayers with FeCo-layers thinner than 1.7–1.8 nm exhibit superparamagnetic behavior (no coercivity and remanence) at room temperature with peak relative low-field permeability up to 887. By exceeding this critical thickness, the neighboring FeCo-aggregates started to coalesce, and this led to the ferromagnetic behavior revealed by a finite coercivity and remanence in the hysteresis loops.

© 2019 Author(s). All article content, except where otherwise noted, is licensed under a Creative Commons Attribution (CC BY) license (<http://creativecommons.org/licenses/by/4.0/>). <https://doi.org/10.1063/1.5079477>

I. INTRODUCTION

Nanoscale magnetic materials have received wide-spread interest in recent years due to their great potential for the development of new generation devices combining the advantages of semiconductor electronics with the spin-selective transport, e.g.

magneto-resistive sensors, ultrahigh density memory cells and high-frequency programmable logic systems.^{1–3} In particular, discontinuous ferromagnetic-insulator multilayers consisting of separated layers of closely spaced ferromagnetic nanoparticles embedded in an insulating matrix have received special attention because the magnetic and transport properties of these structures can be accurately

tuned within a wide range by simply changing the thickness of the ferromagnetic layer.⁴⁻¹²

Enhanced-permeability-dielectrics (EPD) are a particular class of discontinuous ferromagnetic-insulator multilayers¹³ where the magnetic nanoparticles are smaller than the superparamagnetic (SP) limit. These materials have been introduced to reduce the switching field in arrays of single-layer magnetoresistive-random-access-memory (MRAM) bits^{13,14} and the nulling clock field in nanomagnetic logic (NML) systems¹⁵ by increasing the magnetic flux density in the EPD material surrounding these devices.

In this work, we present a study of the structural and magnetic properties of nanoscale FeCo/Al₂O₃-multilayer thin films deposited on 8"-Si wafers in an industrial, high-throughput magnetron sputtering system. We discuss the interdependence between structural and magnetic properties in these materials for FeCo-layer thicknesses in the ~1–2 nm range, where these layers are either discontinuous and/or near the continuous-discontinuous transition regime. Our objective is to fabricate EPD thin films with high magnetic permeability ($\mu_r \gg 1$), no hysteresis, and no remanence, while still retaining their insulating properties.

II. EXPERIMENTAL

We deposited FeCo/Al₂O₃-multilayers on 8"-Si wafers in a high-throughput Evatec LLS-EVO-II batch sputter system (supplementary material).¹⁶⁻²¹ The EPD-multilayers consisted of 25-periods of alternating FeCo-layers with nominal thickness in the 0.5–2nm range deposited by DC sputtering from a Fe₆₀Co₄₀ target, and 3.5nm-thick (nominal) Al₂O₃-interlayers deposited by RF sputtering from an Al₂O₃ target. Since our objective was to produce EPD layers with the highest relative permeability, we selected the Fe₆₀Co₄₀ magnetic alloy for this work because this material has the largest saturation magnetization of any material (~2.45 T).²² Structural properties (e.g. layer thickness, vertical and lateral grain size, separation between the grains) of the FeCo/Al₂O₃-multilayers were investigated by means of grazing-incidence-small-angle-X-ray-scattering (GISAXS), X-ray-reflectivity (XRR), highly-asymmetric-X-ray diffraction (AXRD), non-coplanar grazing-incidence-diffraction (GID) and X-ray-fluorescence (XRF) measurements (supplementary material). The discontinuity of the FeCo-layers was also qualitatively studied by room-temperature magnetic-force-microscopy (MFM) (supplementary material).

The evolution of magnetic properties with the FeCo-layer thickness was first investigated by means of *B-H* hysteresis loop measurements (averaged over the entire 8" wafers) in fields up to 0.1T using a Shb Instruments MESA200 measurement system. Magnetization measurements were then performed with a Quantum Design physical properties measurements (PPMS) setup in fields up to 7T, using a vibrating-sample-magnetometer (VSM) option. Temperature scans of magnetization were performed for both zero-field-cooling (ZFC) and field-cooling (FC) directions. Thus, ZFC measurements were performed by cooling the sample from room temperature to 10K in zero applied magnetic field, and then magnetization was recorded while heating the sample under a 150Oe applied magnetic field. Moreover, magnetic field dependent magnetization measurements were performed at room temperature and at 10K.

III. RESULTS AND DISCUSSION

Owing to the much higher surface energy of FeCo compared to that of Al₂O₃,¹² the FeCo-layers exhibit a granular structure consisting of isotropically distributed nanoclusters as revealed by MFM and GISAXS measurements (see Fig. 1 and supplementary material). It was found that the approximate mean distance *D* between the nanocluster centers increases with the FeCo-layer thickness (Table I), and this can be attributed to the increase of nanoclusters with the FeCo-layer thickness. The individual layer thicknesses of the FeCo/Al₂O₃-multilayers with nominal FeCo-layer thicknesses of 0.5–2nm (samples S1–S4) obtained from XRR measurements (Fig. 2a, b) are summarized in Table I. Thus, the FeCo-layer thicknesses obtained from XRR are in general larger than the nominal ones. To determine the average transversal and lateral grain sizes in the FeCo-layers we performed detector scans in both AXRD and GID geometries (Fig. 2c, d). Figure 2c shows the AXRD patterns (incidence angle $\theta_i=6^\circ$), where the peak at $2\theta=44.7^\circ$ corresponds to (110) crystallographic planes of the bcc-FeCo. For sample S1 the FeCo(110) peak was undetectable, which suggests that the FeCo-layers in this sample are amorphous.

We determined the grain size *d* along an inclined direction with respect to surface normal by ($\theta_i=6^\circ$) using the Scherrer equation $d=0.95\lambda/(FWHM \cdot \cos\theta)$, where $\lambda=0.154\text{nm}$ is the wavelength of X-rays, $\theta=22.35^\circ$, and *FWHM* is the full-width-at-half-maximum in radians, corrected by the resolution function (Table I).²³ Since $t_{XRR} \sim d_{AXRD}$, the FeCo-nanoclusters are limited by the layer thickness in the growth direction. However, in the GID measurements the FeCo(110) diffraction peaks are much sharper, and therefore the grains are larger (Table I). Moreover, it is also observed that the thicker the FeCo-layers the larger the grains, which is consistent with the GISAXS measurements. We have also performed AXRD measurements using a 2D-detector that allows recording the diffraction

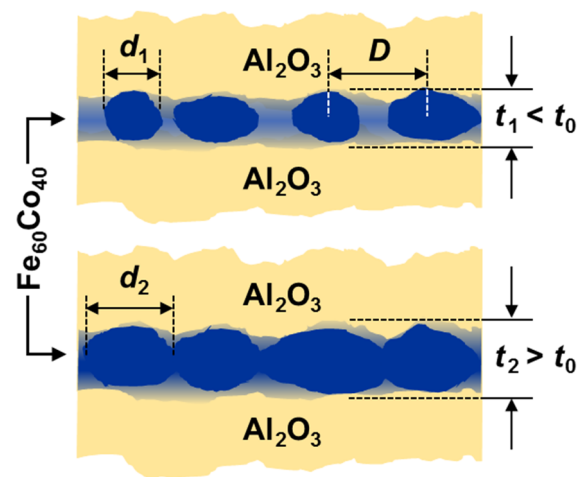


FIG. 1. Growth model of the discontinuous FeCo/Al₂O₃ multilayers. For thicknesses below a certain limit (t_0) the FeCo layers are discontinuous, and above this critical thickness the FeCo particles gradually merge forming quasi-continuous layers; d_1 and d_2 are the average lateral dimensions of the magnetic particles for FeCo layer thickness t_1 and t_2 , respectively, and *D* is the average nearest-neighbor distances between the FeCo nanoclusters.

TABLE I. Structural analysis of $25 \times (\text{FeCo}/\text{Al}_2\text{O}_3)$ -multilayers by various X-ray scattering techniques, where t_{nom} and t_{XRR} are the nominal and experimental layer thicknesses obtained from XRR, d_{AXRD} and d_{GID} are the grain sizes obtained from AXRD and GID measurements, respectively, and D_{GISAXS} is the mean distance between the FeCo-nanoclusters. One should note that d_{AXRD} is determined along a direction inclined with the surface normal by an angle of 12.35° , whereas d_{GID} is determined in the sample plane.

Sample	t_{nom} [nm]		t_{XRR} [nm]		d_{AXRD} [nm]	d_{GID} [nm]	D_{GISAXS} [nm]
	FeCo	Al_2O_3	FeCo	Al_2O_3			
S1	0.5	3.5	1.15 ± 0.10	3.32 ± 0.10	–	–	3.4
S2	1.0	3.5	1.64 ± 0.10	3.37 ± 0.10	1.30 ± 0.10	8.0 ± 1.0	5.5
S3	1.5	3.5	1.85 ± 0.10	3.79 ± 0.10	1.90 ± 0.08	10.5 ± 1.0	7.4
S4	2.0	3.5	2.10 ± 0.10	3.85 ± 0.10	2.30 ± 0.06	12.0 ± 1.0	9.6

signal out of the scattering plane ($\pm 15^\circ$), and as such is also sensitive to texture. Thus, we found out that the FeCo(110) peak at $2\theta=44.7^\circ$ consists of a Debye ring shape (supplementary material), and therefore the FeCo-layers have no preferential orientation in the detecting range.

To get insight into chemical composition of FeCo-layers, we performed incidence angle scans ($2\theta_{impl}=44.7^\circ$) for GID and XRF (Fig. 2e, f), which are depth-sensitive to crystalline material content and chemical composition, respectively.^{24,25} We observe that both GID and XRF profiles exhibit S-shaped kinks for incidence angles corresponding to the positions of superlattice peaks in the XRR patterns, which are due to the standing waves formed inside

the FeCo/ Al_2O_3 -multilayer by the incident and reflected waves. The fitting parameters of the GID profiles were the thicknesses of the FeCo-layers, whereas the XRF profiles were modelled with the Fe and Co concentrations (black lines in Fig. 2e, f). Since the amplitude of the S-shaped kinks in the GID and XRF profiles is different, the crystallinity can vary within the multilayer; in other words, not all Fe and Co atoms that contributed to the XRF profiles are located inside the polycrystalline grains, but they can also diffuse into the Al_2O_3 -matrix. Moreover, the FeCo layers may also contain a certain fraction of Al_2O_3 . For samples S1–S4 in Table I we found that 15%, 12%, 10% and 8% of the Fe and Co atoms have diffused into the Al_2O_3 -matrix with respect to the FeCo-layers.

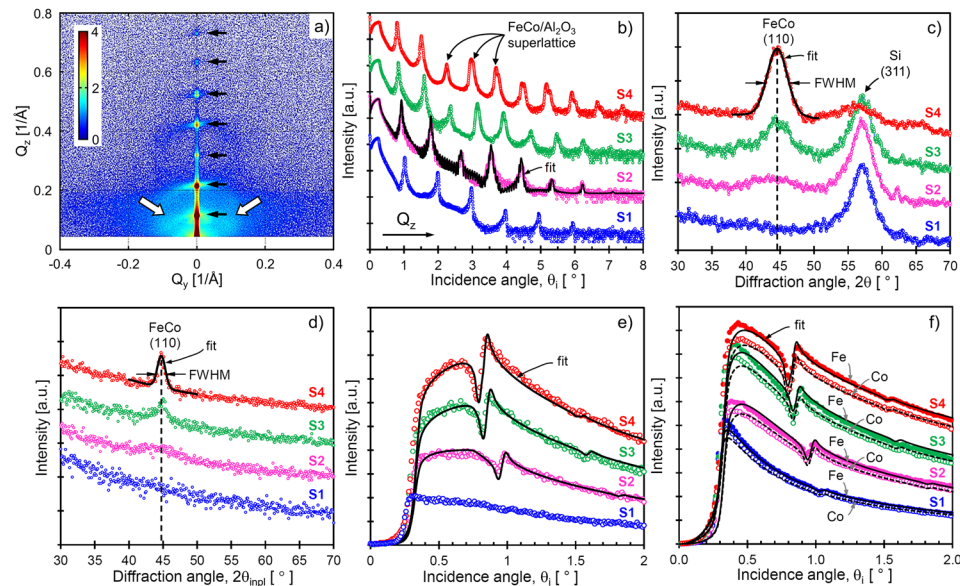


FIG. 2. a) Reflectivity RSM of 25-period FeCo/ Al_2O_3 -multilayer with 2nm-thick (nominal) FeCo-layers (sample S4). The peaks along Q_z -direction for $Q_y=0$ (depicted by black arrows) arise from the constructive interference of X-rays scattered at various buried interfaces. The white arrows indicate the diffused scattering due to the granular FeCo layers. b) Specular XRR scans (shifted vertically for clarity) along Q_z -direction ($Q_y=0$) for samples S1–S4 in Table I. Black line is fit of the XRR pattern for sample S2. c) Detector 2θ -scans (shifted vertically for clarity) in the AXRD scattering geometry for samples S1–S4 (incidence angle $\theta_i=6^\circ$); the black line is a Gaussian fit of the FeCo(110) diffraction peak. d) Detector $2\theta_{impl}$ -scans (shifted vertically for clarity) in the GID geometry for samples S1–S4 (incidence angle $\theta_i=1^\circ$); the black line is a Gaussian fit of the FeCo(110) diffraction peak. e) Incidence angle θ_i -scans (shifted vertically for clarity) in the GID geometry for samples S1–S4 (detector angles $2\theta_{impl}=44.7^\circ$, $\theta_i=1^\circ$). f) Incidence angle θ_i -scans (shifted vertically for clarity) of Fe and Co XRF signals. The black lines in panels (e) and (f) represent fits using the standing wave technique.

Thus, the total intermixing decreases when the FeCo layer thickness increases. Furthermore, by comparing the intensity of the XRF profiles for Fe and Co, after correcting for the different scattering radii of the Fe and Co atoms, we can deduce that the Fe/Co ratio in the FeCo-layers for samples S1 to S4 is $(59 \pm 1)/(41 \pm 1)$, which is agrees very well with the nominal value of the $\text{Fe}_{60}\text{Co}_{40}$ target.

Figure 3 shows temperature dependent magnetization measurements under weak magnetic field for ZFC and FC directions for the $\text{FeCo}/\text{Al}_2\text{O}_3$ -multilayers with FeCo-layer thicknesses ranging from 1.33nm to 2.03nm (measured by XRR). The multilayer with 1.33nm thick FeCo-layers exhibits a clear paramagnetic response (blue curve in Fig. 3a). Increasing the FeCo-layer thickness to 1.42nm leads to formation of magnetic nanostructures, which appear as a thermally relaxed peak on the ZFC curve at 26K (Fig. 3b). Furthermore, the multilayer with 1.56nm thick FeCo-layers also exhibits a thermally relaxed behavior on the ZFC curve at a slightly elevated temperature, 31K (Fig. 3b). We attribute the peaks in the ZFC curves of EPD samples with 1.42nm and 1.56nm thick FeCo-layers to the SP behavior of the discontinuous FeCo-layers.¹³ However, the multilayer with 1.69nm thick FeCo-layers exhibits a broader thermal relaxation compared to the thinner films (Fig. 3b), and this could be assigned to a broader size distribution of the FeCo-nanostructures leading to the existence of both ferromagnetic and SP phases at the same time.

Thermally relaxed SP behavior disappears by further increasing the FeCo-layer thickness (Fig. 3a, b). One can estimate the average magnetic particle volumes (V) from the observed blocking temperatures (T_b) by using the formula $T_b \approx K_u V / 30 k_B$, where K_u is the anisotropy energy of the bulk material, and k_B is the Boltzmann constant.²⁶ Using an anisotropy energy of $0.1\text{MJ}/\text{m}^3$ for $\text{Fe}_{60}\text{Co}_{40}$ alloy,²⁷ the above formula yields average magnetic particle volumes of 25.7nm^3 and 128nm^3 (particle diameters of 3.66nm and 6.25nm if one assumes they are spherical) for the multilayers with nominal FeCo-layer thicknesses of 1.42nm and 1.56nm, respectively. However, since the particles are limited in the growth direction by the layer thickness, they could be more realistically approximated by thin disks with thicknesses of 1.42nm and 1.56nm, and the diameters of 4.8nm and 10.2nm, respectively. These values are consistent with the GID measurements discussed before, where sample S2 with 1.64nm thick FeCo-layers have grains with an average diameter of 8nm. Magnetization of the SP particles above blocking

temperature can be expressed by $M = M_0 L(x)$, where M_0 is the saturation magnetization and $L(x)$ represents the Langevin function with $x = \mu B / k_B T$.²⁸ By fitting the experimental magnetization data with the Langevin equation one can estimate the average magnetic particle volume. Thus, for multilayers with FeCo-layer thicknesses of 1.42nm and 1.56nm one obtains average particle volumes of 25nm^3 and 37nm^3 , respectively. While the first value matches that obtained from T_b , the second one does not. This discrepancy could be attributed to the nature of the Langevin function, which needs further correction for different particle shapes with broader size distribution.²⁹

Room-temperature magnetic-field-dependent magnetization measurements of the $\text{FeCo}/\text{Al}_2\text{O}_3$ -multilayers with FeCo-layer thicknesses (measured by XRR) ranging from 1.33nm to 2.03nm are presented in Fig. 4a. Saturation magnetization scales with the FeCo-layer thickness, and eventually for the thickest layers (1.96nm, 2.03nm) reaches the magnetization values expected for thick ($>50\text{nm}$) FeCo-films.^{30,31} Similar to the magnetic-field-dependent magnetization measurements, magnetic flux densities (B , not shown here) also scale with the FeCo-layer thickness. Due to their higher sensitivity at low fields, we used the B - H hysteresis loop measurements to determine the coercive field (H_c) as a function of layer thickness (Fig. 4d, e). We observe that the multilayers with FeCo-layers below the thickness of 1.74nm exhibit SP behavior (no coercivity and remanence) at room temperature. By exceeding this critical thickness, the multilayers start to gradually exhibit ferromagnetic properties revealed by a finite coercivity and remanence in the hysteresis loops. We also used the B - H hysteresis loops to estimate the magnetic permeability as shown in Fig. 4c, d. The obtained peak magnetic permeability for the $\text{FeCo}/\text{Al}_2\text{O}_3$ -multilayers versus the FeCo-layer thickness at the field $H^* \sim 0.3$ Oe is shown in Fig. 4f, where the sample with 1.33nm-thick FeCo-layers was excluded because it only has a paramagnetic response. Thus, we observe that relative permeability exhibits an increase from 7 to 20 when the thickness of the FeCo-layers increases from 1.42nm to 1.56nm, but then it drops to 5.6 when the thickness is increased to 1.69nm, and this could be due to the formation of larger structures having a ferromagnetic response, as explained above. By further increasing the FeCo-layer thickness, the relative permeability increases rapidly and at 2.03nm it exceeds 10000. These results show that the magnetic properties of the $\text{FeCo}/\text{Al}_2\text{O}_3$ -multilayers are extremely sensitive to the FeCo-layer thickness. Compared to similar EPD thin films based

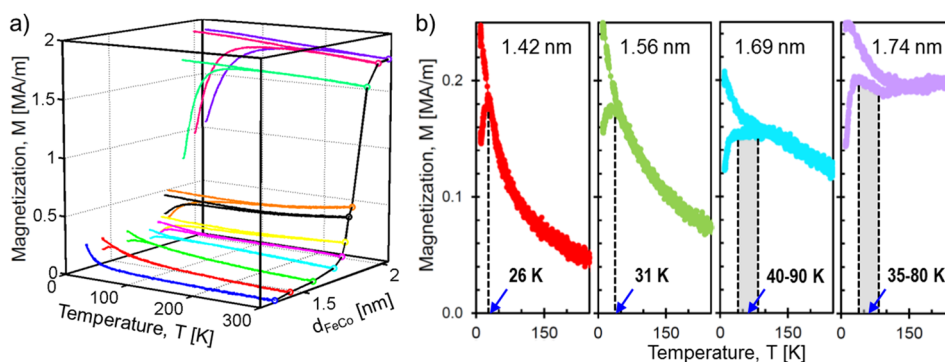


FIG. 3. Temperature-dependent magnetization curves, e.g. zero-field cooled/field cooled (ZFC-FC) measured under a 150 Oe magnetic field for 25-period $\text{FeCo}/\text{Al}_2\text{O}_3$ -multilayers with the FeCo layer thickness (d_{FeCo}) measured by XRR ranging from 1.33nm to 2.03nm. To better observe the behavior of magnetization at low temperatures for the discontinuous multilayers, the ZFC-FC magnetization curves for samples with 1.42nm, 1.56nm, 1.69nm and 1.74nm FeCo-layers are depicted separately, together with the corresponding blocking temperatures.

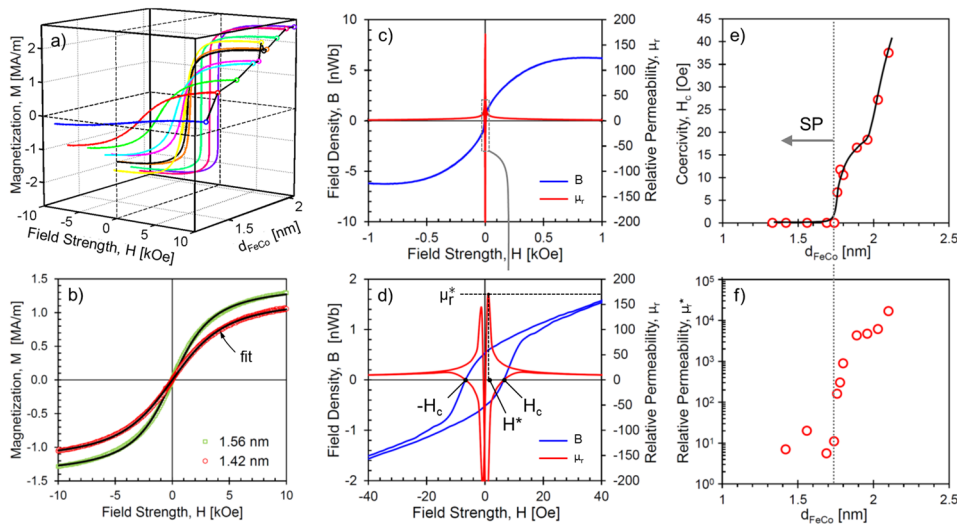


FIG. 4. a) M vs. H hysteresis loops for 25-period $\text{FeCo}/\text{Al}_2\text{O}_3$ -multilayers, with FeCo -layer thickness (d_{FeCo}) ranging from 1.33nm to 2.03nm; b) M vs. H hysteresis loops of the 25-period $\text{FeCo}/\text{Al}_2\text{O}_3$ -multilayers with 1.42nm and 1.56nm-thick (nominal) FeCo -layers; the experimental curves were fitted with Langevin profiles; c) and d) B vs. H and μ_r vs. H for the $\text{FeCo}/\text{Al}_2\text{O}_3$ -multilayer with 1.76nm thick FeCo -layers, where H_c denotes the coercive field, and H^* the field at which the relative permeability is maximum (μ_r^*); e) H_c vs. d_{FeCo} , where the continuous line mimics the trend of the data; f) μ_r^* vs. d_{FeCo} . The dotted line in (e) and (f) at $d_{\text{FeCo}}=1.74\text{nm}$ defines the transition between superparamagnetic (SP) and ferromagnetic behaviors.

on FeCo and Al_2O_3 reported in literature, our $\text{FeCo}/\text{Al}_2\text{O}_3$ multilayers exhibit substantially higher relative permeabilities for similar FeCo -layer thicknesses.^{13,15}

IV. CONCLUSIONS

In summary, we deposited nanostructured $\text{FeCo}/\text{Al}_2\text{O}_3$ -multilayers in an industrial, high-throughput Evatec LLS EVO II magnetron sputtering system. By performing a thorough X-ray scattering analysis we revealed the granular structure of the FeCo -layers, which evolves from isolated nanoparticles towards continuous layers with increasing layer thickness. Magnetic measurements showed that the multilayers with FeCo -layers below the thickness of 1.74nm exhibited superparamagnetic behavior (no coercivity and remanence) at room temperature, and by exceeding this critical thickness, the neighboring FeCo -islands started to coalesce, and this led to the ferromagnetic behavior revealed by a finite coercivity and remanence in the hysteresis loops.

SUPPLEMENTARY MATERIAL

See [supplementary material](#) for details on the LLS EVO II sputter tool, and X-ray scattering and MFM experiments.

ACKNOWLEDGMENTS

We are grateful to Marco Padrun, Albert Koller, Silvan Wuethrich, Roland Rettenmeier, Maurus Tschirky, Thomas Nadig and Martin Bless for continued support, Jean-Philippe Michel and Josef Zweck for scientific discussions, and the Nanoscale Materials Science Lab at Empa for providing access to their facilities. We also acknowledge financial support from the Swiss Federal Commission for Technology and Innovation (CTI-Project Nr. 18940.2 PFNM-NM). The work was partially supported by CEITEC Nano Research Infrastructure (ID LM2015041, MEYS CR, 2016–2019) and by the MEYS of the Czech Republic under the project CEITEC 2020 (LQ1601).

REFERENCES

- G. A. Prinz, *Science* **282**, 1660 (1998).
- S. A. Wolf, D. D. Awschalom, R. A. Buhrman, J. M. Daughton, S. von Molnár, M. L. Roukes, A. Y. Chtchelkanova, and D. M. Treger, *Science* **294**, 1488 (2001).
- A. Ney, C. Pampuch, R. Koch, and K. H. Ploog, *Nature* **425**, 485 (2003).
- B. Dieny, S. Sankar, M. R. McCartney, D. J. Smith, P. Bayle-Guillemaud, and A. E. Berkowitz, *J. Magn. Magn. Mater.* **185**, 283 (1998).
- G. N. Kakazei, P. P. Freitas, S. Cardoso, A. M. L. Lopes, M. M. Pereira de Azevedo, Yu. G. Pogorelov, and J. B. Sousa, *IEEE Trans. Magn.* **35**, 2895 (1999).
- G. N. Kakazei, Yu. G. Pogorelov, A. M. L. Lopes, J. B. Sousa, S. Cardoso, P. P. Freitas, M. M. Pereira de Azevedo, and E. Snoeck, *J. Appl. Phys.* **90**, 4044 (2001).
- W. Kleemann, O. Petravic, Ch. Binek, G. N. Kakazei, Yu. G. Pogorelov, J. B. Sousa, S. Cardoso, and P. P. Freitas, *Phys. Rev. B* **63**, 134423 (2001).
- G. N. Kakazei, Yu. G. Pogorelov, J. A. M. Santos, J. B. Sousa, P. P. Freitas, S. Cardoso, N. A. Lesnik, and P. E. Wigen, *J. Magn. Magn. Mater.* **266**, 57 (2003).
- M. Anas, C. Bellouard, and M. Vergnat, *J. Appl. Phys.* **96**, 1159 (2004).
- R. Bručas, M. Hanson, P. Apell, P. Nordblad, R. Gunnarsson, and B. Hjörvars-son, *J. Appl. Phys.* **101**, 073907 (2007).
- H. Silva, H. L. Gomes, Yu. G. Pogorelov, P. Stallinga, D. M. de Leeuw, J. P. Araujo, J. B. Sousa, S. C. J. Meskers, G. Kakazei, S. Cardoso, and P. P. Freitas, *Appl. Phys. Lett.* **94**, 202107 (2009).
- H. G. Silva, A. M. Pereira, J. M. Teixeira, J. M. Moreira, G. N. Kakazei, J. P. Araújo, Yu. G. Pogorelov, J. B. Sousa, M. E. Braga, B. Raquet, H. Rakoto, C. Gatel, E. Snoeck, S. Cardoso, and P. P. Freitas, *Phys. Rev. B* **82**, 14432 (2010).
- S. V. Pietambaram, N. D. Rizo, R. W. Dave, J. Goggin, and K. Smith, *Appl. Phys. Lett.* **90**, 143510 (2007).
- S. V. Pietambaram, N. D. Rizo, and J. M. Slaughter, US7683445B2 (2010).
- P. Li, V. K. Sankar, G. Csaba, X. S. Hu, M. Niemier, W. Porod, and G. H. Bernstein, *IEEE Trans. Magn.* **48**, 3292 (2012).
- <https://www.evatecnet.com/products/lls-evo-ii>.
- C. V. Falub, H. Rohrmann, M. Bless, M. Meduña, M. Marion, D. Schneider, J. H. Richter, and M. Padrun, *AIP Advances* **7**, 056414 (2017).
- C. V. Falub, R. Hida, M. Meduña, J. Zweck, J.-P. Michel, H. Sibuet, D. Schneider, M. Bless, J. H. Richter, and H. Rohrmann, *IEEE Trans. Magn.* **53**(11), 2002906 (2017).
- C. V. Falub, M. Bless, R. Hida, M. Meduña, and A. Ammann, *AIP Advances* **8**, 048002 (2018).

- ²⁰R. Hida, C. V. Falub, S. Perraudeau, C. Morin, S. Favier, Y. Mazel, Z. Saghi, and J.-P. Michel, *J. Magn. Magn. Mater.* **453**, 211 (2018).
- ²¹J.-P. Michel, H. Sibuet, N. Buffet, J.-C. Bastien, R. Hida, B. Viala, P. Poveda, A.-S. Berneux-Dugast, E. Bruno, and C. V. Falub, *IEEE Trans. Magn.* (submitted).
- ²²F. M. Bozorth, *Ferromagnetism* (IEEE Press, New York, 1993), pp. 190–209.
- ²³B. D. Cullity and S. R. Stock, *Elements of X-Ray Diffraction*, 3rd ed. (Prentice-Hall Inc., 2001), pp. 167–171.
- ²⁴*The X-Ray Standing Wave Technique: Principles and Applications*, edited by J. Zegenhagen and A. Kazimirov (World Scientific, 2013).
- ²⁵J. Krcmar, V. Holy, and I. Vavra, *Appl. Phys. Lett.* **94**, 101909 (2009).
- ²⁶O. Yildirim, S. Cornelius, A. Smekhova, G. Zykov, E. A. Gan'shina, A. B. Granovsky, R. Hübner, C. Bähz, and K. Potzger, *J. Appl. Phys.* **117**, 183901 (2015).
- ²⁷T. Mühge, T. Zeidler, Q. Wang, C. Morawe, N. Metoki, and H. Zabel, *J. Appl. Phys.* **77**, 1055 (1995).
- ²⁸S. D. Tiwari and K. P. Rajeev, *Sol. State Commun.* **152**, 1080 (2012).
- ²⁹M. El-Hilo, *J. Appl. Phys.* **112**, 103915 (2012).
- ³⁰V. A. Vas'ko, V. R. Inturi, S. C. Riemer, A. Morrone, D. Schouweiler, R. D. Knox, and M. T. Kief, *J. Appl. Phys.* **91**, 6818 (2002).
- ³¹Y. Fu, T. Miyao, J. W. Cao, Z. Yang, M. Matsumoto, X. X. Liu, and A. Morisako, *J. Magn. Magn. Mater.* **308**, 165 (2007).